

https://dspace.org/

Environmental impacts of shifts in surface urban heat island emissions and nighttime light during the RussiaUkraine war in Ukrainian cities

G Roshan; A Ghanghermeh; R Sarli; Stefan Grab

SPRINGER HEIDELBERG
https://hdl.handle.net/10539/41482
WOS

Downloaded from a DSpace repository. https://dspace.org/

Environmental Science and Pollution Research (2024) 31:45246–45263
https://doi.org/10.1007/s11356-024-34050-x

RESEARCH ARTICLE

Environmental impacts of shifts in surface urban heat island, emissions, and nighttime light during the Russia–Ukraine war in Ukrainian cities

Gholamreza Roshan[1] · Abdolazim Ghanghermeh[1] · Reza Sarli[2] · Stefan W. Grab[3]

Received: 18 January 2024 / Accepted: 16 June 2024 / Published online: 4 July 2024
© The Author(s), under exclusive licence to Springer-Verlag GmbH Germany, part of Springer Nature 2024

Abstract

As recent geopolitical conflicts and climate change escalate, the effects of war on the atmosphere remain uncertain, in particular in the context of the recent large-scale war between Russia and Ukraine. We use satellite remote sensing techniques to establish the effects that reduced human activities in urban centers of Ukraine (Kharkiv, Donetsk, and Mariupol) have on Land Surface Temperatures (LST), Urban Heat Islands (UHI), emissions, and nighttime light. A variety of climate indicators, such as hot spots, changes in the intensity and area of the UHI, and changes in LST thresholds during 2022, are differentiated with pre-war conditions as a reference period (i.e., 2012–2022). Findings show that nighttime hot spots in 2022 for all three cities cover a smaller area than during the reference period, with a maximum decrease of 3.9% recorded for Donetsk. The largest areal decrease of nighttime UHI is recorded for Kharkiv (− 12.86%). Our results for air quality changes show a significant decrease in carbon monoxide (− 2.7%, based on the average for the three cities investigated) and an increase in Absorbing Aerosol Index (27.2%, based on the average for the three cities investigated) during the war (2022), compared to the years before the war (2019–2021). The 27.2% reduction in nighttime urban light during the first year of the war, compared to the years before the war, provides another measure of conflict-impact in the socio-economic urban environment. This study demonstrates the innovative application of satellite remote sensing to provide unique insights into the local-scale atmospheric consequences of human-related disasters, such as war. The use of high-resolution satellite data allows for the detection of subtle changes in urban climates and air quality, which are crucial for understanding the broader environmental impacts of geopolitical conflicts. Our approach not only enhances the understanding of war-related impacts on urban environments but also underscores the importance of continuous monitoring and assessment to inform policy and mitigation strategies.

Keywords War · Urban climate · Satellite remote sensing · Environmental impact · Climate feedback

Introduction

Recent times have seen escalated socio-political tensions across several regions globally. We are arguably living in one of the most politically sensitive times in recent world history, such that even climate change has been affected by the micro- and macro-policies of governmental and international actors (Watts and Conger 2022; Mortoja and Yigitcanlar 2022; Asfew et al. 2023; Apraku et al. 2023; Söder 2023). Climate response to politically charged human activities is not only limited to the performance of governments during times of relative peace but also the military performance and war between countries, which may irreparably impact climate (Selby 2019; Burnett and Mach 2021; Jayaram and Brisbois 2021; Garfin et al. 2021; Sovacool et al. 2023; Garajeh et al. 2024). For instance, atmospheric air pollution

Responsible Editor: Rongrong Wan

✉ Gholamreza Roshan
ghr.roshan@gu.ac.ir; r.rowshan@yahoo.com

[1] Department of Geography, Golestan University, Shahid Beheshti, Gorgan 49138-15759, Iran

[2] Department of Forest Resources Management, Faculty of Forestry, University of Agriculture in Krakow, AL. 29 Listopada 46, 31-425 Kraków, Poland

[3] School of Geography, Archaeology and Environmental Studies, University of the Witwatersrand, Private Bag 3, Wits, Johannesburg 2050, South Africa

significantly increased due to the long-range transport of organic pollutants during the Kosovo War (Vukmirović et al. 2001), and high levels of gaseous pollutants and particulate matter were identified in association with the oil fires during the Persian Gulf War (Husain 1998). Climate change and hazards have a close and two-way relationship with political and military conflicts, such that they may directly impact each other (Qin et al. 2023; Buhaug et al. 2023). For instance, the effects of climate change on prolonging and intensifying droughts can lead to cross-border disputes over the control of essential resources, such as water (Donnelly et al. 2012; Gleick 2019; Schillinger et al. 2022; Shumilova et al. 2023). Conversely, the destructive impacts of war may have direct consequences on the natural environment (e.g., atmospheric chemistry; pollution of water resources; burnt vegetation) and even influence climate change (e.g., Herndon 2019).

On 24 February 2022, Russia attacked Ukraine from several fronts. Attacks on civilian and military sites have caused air, land, and water pollution, especially in the heavily industrialized country of Ukraine (Rawtani et al. 2022; Pereira et al. 2022). Buildings destroyed by the war in Ukraine have been emitting carcinogenic dust for decades (Neckel et al. 2022; United Nations Environment Programme 2022). Heavy metals and chemicals have seeped into groundwater, poisoning water supplies and killing aquatic life in rivers and water bodies (United Nations Environment Programme 2022; Shumilova et al. 2023). The conflict has destroyed large tracts of agricultural land, burned forests, and destroyed national parks (Prins 2022; Kordi & Yousefi 2022; Mansourihanis et al. 2023; Sirizi et al. 2023). Damage to industrial facilities has caused severe air, water, and soil pollution and has exposed residents to toxic chemicals and contaminated water (Ramírez and Durón, 2022; Racioppi et al. 2022; Khosravian et al. 2024; Zhang et al. 2023). According to Ukraine's Ministry of Environmental Protection and Natural Resources, about 30% of the country's protected areas, which cover 3 million hectares, have been bombed, polluted, burned, or hit by military maneuvers. Some of the fiercest fighting of the war took place in the forests along the Donets River in the east (Yale Environment 360, 2022). Satellite monitors detected more than 37,000 fires in the first 4 months of the invasion, affecting nearly a quarter of a million hectares of forests and other natural ecosystems (Yale Environment 360, 2022). Thus far, the war has directly led to over 33 million tons of greenhouse gas emissions, which inevitably adds to atmospheric warming (BBC News 2022). Possibly less well understood or investigated is the war's impact on local urban climate. Important attributes of urban climate include Land Surface Temperatures (LST), Urban Heat Islands (UHI), and air pollution, which to a large extent are controlled by the dynamics of daily urban activities (Zhou et al. 2014; Morris et al. 2017; Mahmoud and Gan 2018; Correia Filho et al. 2019; Bilal et al. 2021).

UHIs are areas in cities that have relatively or abnormally high temperatures compared to other areas of the city (Kumar et al. 2023). UHIs are influenced by both local (natural) climatic parameters and human-induced factors related to urban development and activities. Climate factors include solar radiation, wind velocity and direction, cloud cover, soil and air humidity, precipitation, latitude, seasonality, topography, and distance from water bodies (Hathway and Sharples 2012; He BJ 2018; Lin et al. 2020; Ngarambe et al. 2021). Although these factors are almost uncontrollable in existing cities, they are very important for deciding the location of new cities or determining the direction of future city expansion. More controllable climatic factors are those related to the design and construction of the city. For example, the quality of vegetation in the city, land use, urban density, the type of materials used on the exterior of buildings and streets, the shape and geometry of urban structures (which collectively impact incoming solar radiation and energy dispersal), heat absorption/reflection, and airflow (Kooreman et al., 2020; Correia Filho et al. 2021; Ma et al. 2022; Husni et al. 2022; da Silva Espinoza et al. 2023; Hou et al. 2023). Significant changes in the thermal budget of cities may arise through relatively rapid and dramatic changes in human activities. Examples of this have recently been published, demonstrating how urban "lock-downs" or much reduced urban activity (vehicular and air traffic, industrial output) associated with the global coronavirus disease 2019 (COVID-19), have in places improved air quality (e.g., Rodríguez-Urrego & Rodríguez-Urrego 2020; Beria and Lunkar 2021; Nemati et al. 2020; Rudke et al. 2023) and decreased urban heat budgets, hence reducinzg the effects of UHIs (Parida et al. 2021; Kenawy et al. 2021; Jamei et al. 2022; Jallu et al. 2022; Roshan et al. 2022; Mijani et al. 2023). Similarly, it may be expected that outmigration from cities and reduced urban activity during times of war, will have an impact on the urban climate. Our aim is to test this, using the recent Russia-Ukraine war as our case study. We investigate how this war has impacted the urban climates (UHI, LST in particular, and quality air) of Donetsk, Mariupol, and Kharkiv (Fig. 1).

To better highlight the innovative aspects and significance of this study, it is important to emphasize the unprecedented nature of investigating urban climate changes in the context of an ongoing war. This study bridges a critical gap by combining environmental science with geopolitical analysis, offering new insights into how extreme socio-political events can rapidly alter urban microclimates. By focusing on urban heat islands and land surface temperatures, this research not only contributes to urban climate science but also provides essential data that could inform future urban planning and resilience strategies in conflict zones. The use

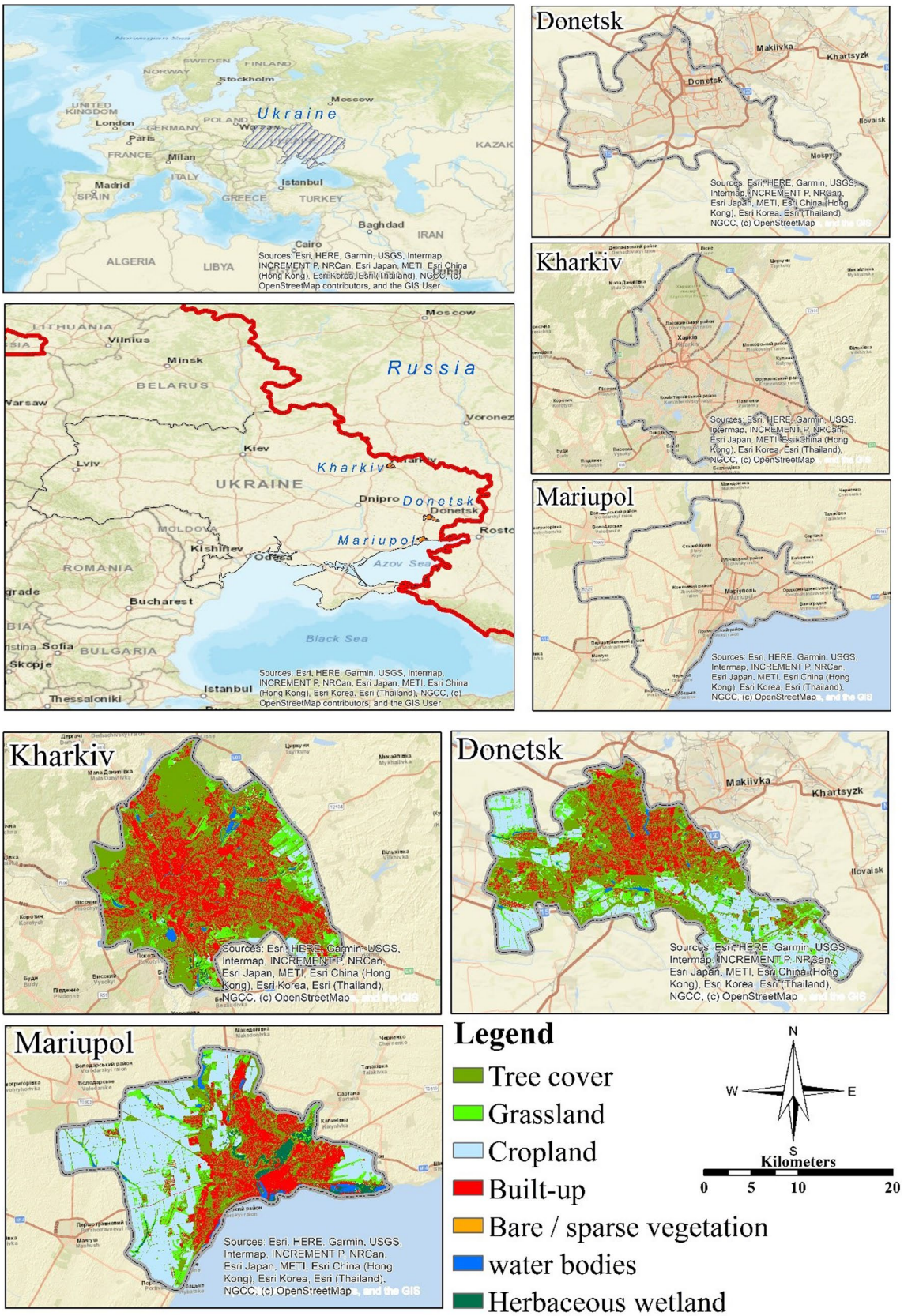


Fig. 1 Land use maps and locations of the three Ukrainian cities: Donetsk, Kharkiv, and Mariupol (ESA World Cover 10 m 2022 v200)

of satellite monitoring and advanced modeling techniques in a war-affected region underscores the innovative methodological approach of this study, which can be replicated in other conflict zones globally.

In summary, this research seeks to understand the broader implications of war on urban environments, emphasizing the need for interdisciplinary approaches to address complex global challenges.

Local setting, materials, and methods

The spatial context of urban destruction in the three cities is presented in Fig. 2 and is based on a report by the United Nations Satellite Center (UNOSAT) (unitar.org, 2022). UNOSAT prepared images for different parts of the cities and for specific dates, upon which the extent of destruction could be determined, together with onsite validation. It is important to note that the results presented in Fig. 2 do not represent the full extent of destruction for the entire urban areas investigated and are only representative for a given point in time (i.e., the results depicted would have changed through ongoing time). For example, it is possible that where only two images are available for a given city, only portions of the city are covered. Figure 2 only shows areas of complete destruction, not partial destruction. On this basis, Fig. 2 indicates completely destroyed areas of Kharkiv, based on a video report dated 24 April 2022 and 21–23 March 2022, and for Donetsk, a similar report dated 26 and 28 March 2022. The spatial pattern of destruction in Mariupol is based on combined results from several image reports (23 and 26 March 2022, 1, 3, 5, 25, and 28 April 2022, and 15 June 2022).

Remote sensing data for establishing hot spot analysis

The MOD11A1 V6.1 product is a daily global surface temperature product derived from the MODIS instrument onboard NASA's Terra satellite. With a spatial resolution of 1000 m and daily temporal resolution since 2012, it has served to monitor and analyze land surface temperature trends and variability and help determine climate change impacts, thus making it an important component of the Land Data Assimilation System (LDAS). Although our initial LST data had a resolution of 1000 m, it was downscaled to 500 m based on the code written on the Google Earth Engine

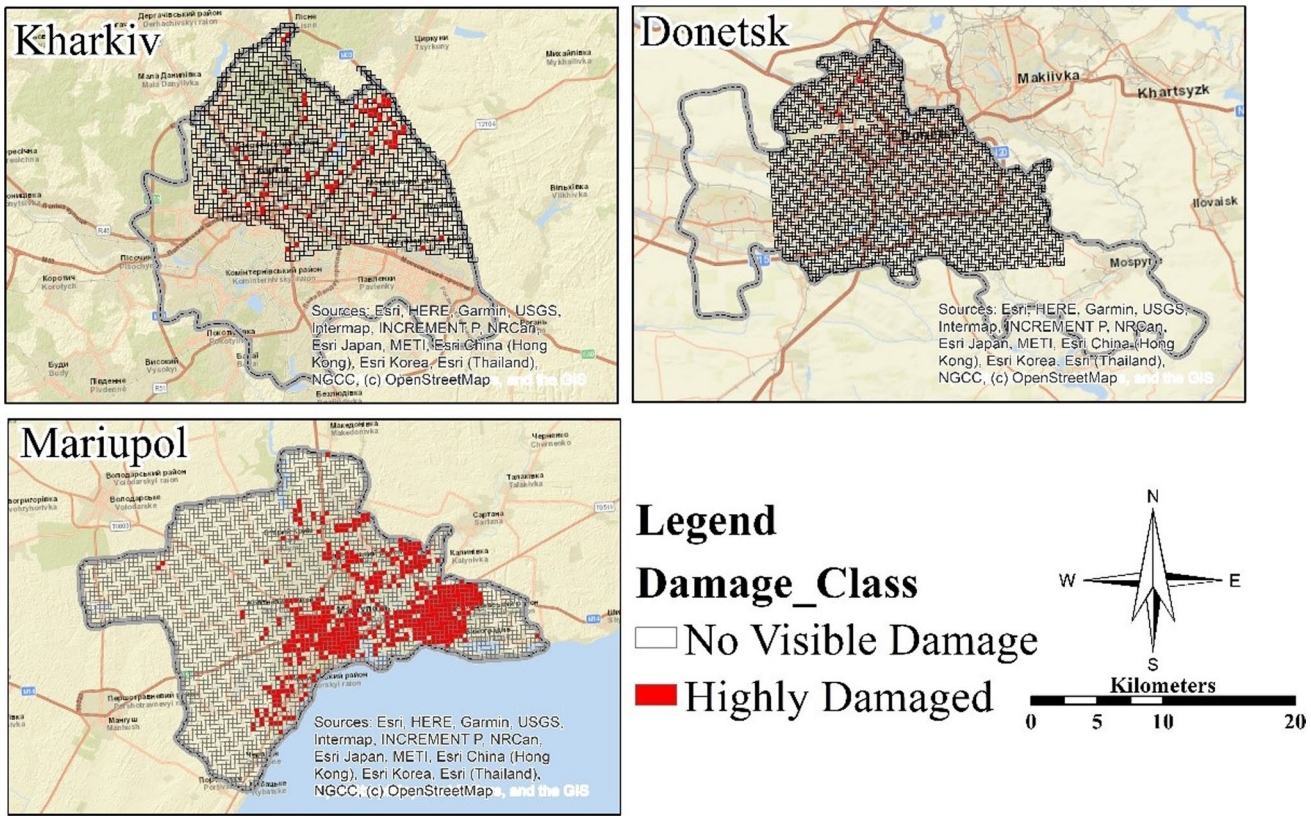


Fig. 2 Damaged areas of Ukrainian cities due to attacks and invasions by Russian forces, based on the UNOSAT report for selected dates (UNOSAT, 2022)

platform. We used the MOD11A1 V6.1 product to perform a hot spot analysis using nighttime data.

To complete and implement a spatial analysis of temperature, the Spatial Statistics Tools section of the Mapping Clusters subset (Getis-Ord Gi) is used. Hot spot analysis, which entails calculating the Getis-Ord $G*I$ statistic for air temperature, was used in the Arc GIS software V.10.8. The $G*i$ value is a z-score indicating where high or low values are clustered. For a hot spot to be statistically significant, a specific location should have a high value and be surrounded by high values. The Getis-Ord is calculated as follows (ESRI 2018; Roshan et al. 2022):

$$G_i^* = \frac{\sum_{j=1}^{n} W_{i,j} - x\sum_{j=1}^{n} W_{i,j}}{s\sqrt{\frac{n-\sum_{j=1}^{n} W_{i,j}^2 - (\sum_{j=1}^{n} W_{i,j})^2}{n-1}}} \quad (1)$$

where i is the resultant G_i^* statistics (z-scores and p values) for pixel i, xj is the LST value for pixel j, wi,j is the spatial weight between pixel i and neighboring pixel j, n is equal to the total number of pixels, and $\overline{X}$ and S are mean and variance:

$$\overline{X} = \frac{\sum_{j=1}^{n} x_j}{n} \quad (2)$$

and

$$S = \sqrt{\frac{\sum_{j=1}^{n} x_j^2}{n} - \left(\overline{X}\right)^2} \quad (3)$$

The G_i^* statistic (z-score) output represents the statistical significance of clustering for a specified distance (ESRI 2018). The z-score was then compared with a range of values using seven confidence levels (Table 1): − 0.01 (values ≤ 2.58); − 0.05 (values ranging from − 2.58 to − 1.96); − 0.1 (values ranging from − 1.96 to − 1.65); 0 (values ranging from − 1.65 to 1.65); 0.1 (values ranging from 1.65 to 1.96); 0.05 (values ranging from 1.96 to 2.58); and 0.01 (values > 2.58). The seven levels correspond to seven classes that LST values were assigned to. These are most important for analyzing "very cold spots" and "very hot spots," which define areas with extreme values. In this study, we only consider nighttime hot and cold spots.

Table 1 Classification based on p value and z-score (Georgiana and Uritescu 2018; Roshan et al. 2021)

Significance level (p value)	Critical value (z-score)	Class No	Class name
− 0.01	≤ 2.58	1	Very cold spot
− 0.05	− 2.58 to − 1.96	2	Cold spot
− 0.10	− 1.96 to − 1.65	3	Cool spot
0	− 1.65 to 1.65	4	Not significant
0.10	1.65 to 1.96	5	Warm spot
0.05	1.96 to 2.58	6	Hot spot
0.01	> 2.58	7	Very hot spot

Establishing the intensity of UHIs

To establish the intensity of UHIs, two indicators were used. The first is to calculate the average temperature for all areas with a z-score > 2.58. The G^*_i statistic has different z-scores. Areas with a z-score > 2.58 are introduced as hot spots, with the highest level of significance = 99%. Temperature differences for urban areas were calculated and compared with the overall average for the suburbs (urban fringe—referred to as "rural"). This method is introduced using the abbreviation G_i^*UHII:

$$Gi^*\text{UHII} = \overline{\text{LST}}_{Z_{2.58}} - \overline{\text{LST}}_{\text{Rural}} \quad (4)$$

In Eq. (4), Gi^*UHII is the UHII index, $\overline{\text{LST}}_{Z_{2.58}}$ is the overall average LST of areas with z-score > 2.58 and $\overline{\text{LST}}_{\text{Rural}}$ is the overall average LST for rural areas. For the second method, the temperature difference between the temperature of each pixel (LST_{P_i}), compared to the overall average temperature of the countryside (village), $\overline{\text{LST}}_{\text{Rural}}$, is calculated. An output is then extracted for each pixel, upon which mapping is also undertaken. This method is introduced using the abbreviation urban heat island intensity per pixel (UHIIP):

$$\text{UHII}P = \text{LST}_{P_i} - \overline{\text{LST}}_{\text{Rural}} \quad (5)$$

Due to human-engineered structures and infrastructure, temperatures of UHIs are significantly higher than those for surrounding rural areas. This is a consequence of urban areas being unable to absorb and radiate heat in the same way that rural areas are able to. For urban citizens, it is thus important to carefully consider where to take up residence, given that the effects of the UHI are spatially variable. In our analysis, we consider it beneficial to select suburbs of similar size and population density to establish the effects of conflict on UHIs. Suburban boundaries may be identified in accordance with high clusters (density) of urban structures representing urban centers. In so doing, we identified a distance of 3 km from the city boundary to define the spatial context of suburbs. During nighttime, the UHI effects become more evident due to the greater thermal inertia of the materials used in urban fabric (Arellano and Roca 2021), Therefore, in this study, we only consider UHI during the night.

Satellite data and air quality determination

Air quality is only determined through satellite data, as ground monitoring stations have for the most part been destroyed and/or it has been impossible to obtain station data since the start of the war. We use the TROPOMI instrument on board the Sentinel-precursor (S5P) to establish the concentration columns (μmol m^{-2}) of gases and particulate matter. Pollutants captured and measured include CO and UVAI_AAI (UV Aerosol Index (UVAI)/ Absorbing Aerosol Index (AAI)) (Zalakeviciute et al. 2020). The UV aerosol index (UVAI) provides a measure of aerosol absorption (Ali et al. 2014; Hammer et al. 2016). We use the TROPOMI offline level 2 AER_AI absorbing aerosol index product from the 340 nm/380 nm (Kooreman et al. 2020). Our study period includes the first year of the war (2022) and 3 years before the war (2019–2021) as a reference period. Daily satellite data were obtained for each city over these periods of time, upon which concentrations of atmospheric pollutants (CO and AAI) were calculated.

Satellite data and analysis for nighttime light

The US Defense Meteorological Satellite Program (DMSP) has developed an Operational Linescan System (OLS) with the aim to remotely measure the faint reflection of moonlight by clouds at night and to obtain the inversion of nighttime meteorological data (Huang et al. 2023). The Day/Night Band (DNB) on the VIIRS sensor, onboard the Suomi National Polar-Orbiting Partnership (Suomi-NPP) and NOAA-20 satellites, is a panchromatic band that is able to detect very dim nighttime scenes (Wang et al., 2017). To this end, we use the VIIRS Stray Light Corrected Nighttime Day/Night Band Composites Version 1 Average DNB radiance values product from the milliJoules per square meter (MJ m^{-2}) (Elvidge et al. 2017). The annual average nighttime light for each urban pixel was calculated, based on total pixels over a given urban area. An overall average pixel value was then calculated for each year, as per the time periods mentioned for air quality data.

A particular value of OLS is its ability to capture urban light during clear nights (Croft 1978; Deren and Xi 2015; Huang et al. 2023). This has led to several nighttime light remote sensing applications for studies assessing urbanization (e.g., Chen et al. 2023), population change (e.g., Wu et al. 2023), economic activity (e.g., Guo et al. 2020; Chen et al. 2023), conflict assessment (e.g., Huang et al. 2023), greenhouse gas emissions, and the environment (e.g., Zhang et al. 2020; Li et al. 2023). Of further value using OLS is the provision of a sense of ongoing socio-economic (human) activity in war-torn urban regions, for which information may otherwise be difficult to come by. It may help establish which parts of a city still have electricity, or conversely, establish the extent of economically damaged areas without electricity. Ultimately, multi-temporal night-time light can provide initial scientific information for purposes of recovery, areas of targeted humanitarian aid, and post-disaster reconstruction efforts (Qiang et al. 2020). The specifications of the VIIRS day/night band (DNB) sensor are presented in Table 2.

Results

Analysis of nighttime hot spots and urban heat islands

Values of − 1 to − 3 (1 to 3) have been identified as cold (hot) points, with significant changes of between 90 and 99% recorded (Table 1). For the city of Kharkiv, the percentage area of cold and hot classes for the reference period (2012–2022) is 23.53 and 24.26%, respectively, during the night (Figs. 3b and 6). Hot and cold spots in 2022 had decreased to 21.78 and 20.76%, respectively (Figs. 3a and 6).

The spatial distribution pattern of hot spots for the reference period is represented by two zones and the main belt, which occurs over the western half of the city. Although this belt has a north–south (N-S) extension, it is more evident over northern than southern parts. Over the eastern half, the north–south belt has expanded, while its primary impact is visible over the southern half (Fig. 3b). During 2022, there is a distribution of hot spots over both western and eastern districts; however, the primary difference with the reference period is that the main area of hot spots in western Kharkiv is over southern parts. Eastern Kharkiv has scattered cores of

Table 2 Specifications of the VIIRS sensor Day/Night Band (DNB) (after Mills et al. 2013; Elvidge et al. 2017, 2021)

Specifications	
Delivery file type	(*.tif) Internal DEFLATE compressed GeoTIFF(*.gz) Gzipped GeoTIFF
Delivery file content	avg_rade9h, cf_cvg, cvg
Delivery file config	vcm, vcmsl
Unit	(avg_rade9h) nW/cm^2/sr
Image file type	GeoTIFF
Image CRS	EPSG:4326 (geographic latitude/longitude)
Image resolution	15 arc-sec (~ 500 m at the Equator)

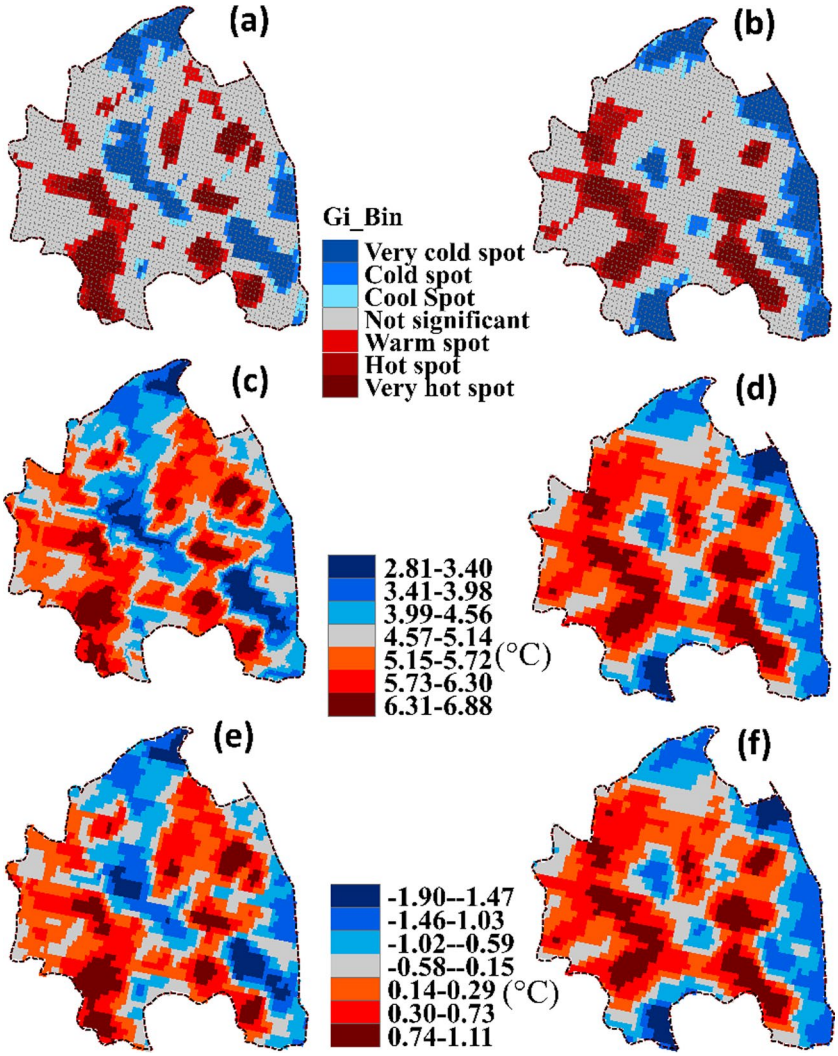


Fig. 3 Spatio-temporal distribution of hot spot analysis: **a** nighttime 2022, **b** nighttime reference period (LST), **c** nighttime 2022, **d** nighttime reference period and urban heat island intensity, **e** nighttime 2022, and **f** nighttime reference period for Kharkiv

hot spots in 2022, in contrast to the more spatially continuous hot spots during the pre-war years. The location of cold spots also differs between 2022 and the reference period. Although the highest concentration of cold spots occurred over the eastern periphery regions of the city during the reference period, this shifted to a greater concentration of cold spots over the central parts of the city in 2022. In addition, we note a cold core over the southern parts of the city for the reference period, which disappears in 2022 but is characterized by warm cores over immediate neighboring areas (Fig. 3a, b).

The LST ranges by between 5 and 8°C during the reference period, while for 2022, it ranges between 4.5 and 8.5°C. For the reference period, the maximum area (40%) has a temperature class of 6.5–7°C, and in 2022, the maximum area (36.5%) has a temperature class of 6–6.5°C (Fig. 3c, d). The curve for 2022 is more positively skewed, indicating lower-than-normal temperatures (Fig. 7).

Variations in the intensity of the heat island may change due to a variety of local and extra-local factors. According to the G_i^*UHII method, the intensity of the heat island in 2022 is greater than that during the reference period. The UHII for the reference period and for 2022 were 1.18 and 1.37°C, respectively.

Significant differences in the urban heat island are observed between the reference period and that of 2022. For the reference period, areas that experienced a decrease and increase in temperature (UHII) is 17 and 83%, respectively, while in 2022, areas that decreased represented 29.86% and areas of increased temperature 70.15% (Fig. 8). For both study periods, the maximum decrease in temperature is observed over eastern, northern, and central areas of the city, while areas of increased UHII were patchy over some eastern and western parts of the city (Fig. 3e, f). The findings of this section show that among the investigated cities, Kharkiv has experienced the largest area decrease in UHII (12.86% decrease) during the night (Fig. 8).

For Donetsk city, the total area of significant cold and hot classes (significance > 90%) as a night average for the

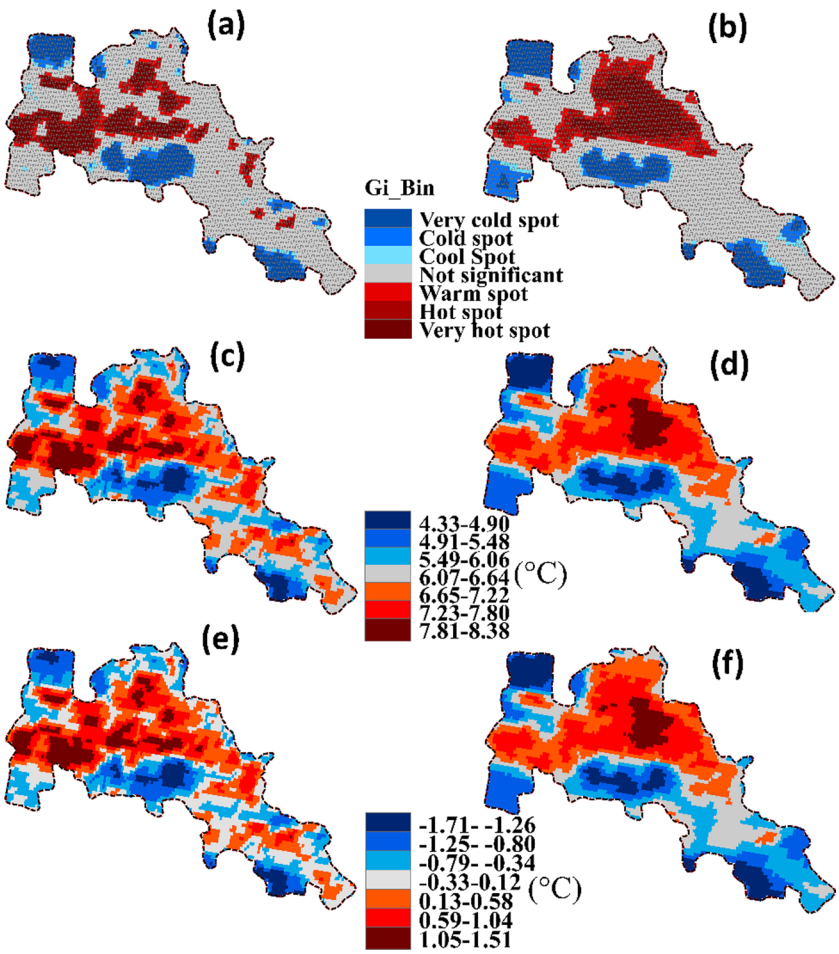


Fig. 4 Spatio-temporal distribution of hot spot analysis: **a** nighttime 2022, **b** nighttime reference period (LST), **c** nighttime 2022, **d** nighttime reference period and urban heat island intensity, **e** nighttime 2022, and **f** nighttime reference period for Donetsk

reference period, were 22.2 and 26.5% of the total city area, respectively (Figs. 4b and 6). The area of cold spots was 22.2%, representing a smaller area compared to hot spots, which occupied 26.5% (Figs. 4b and 6). For 2022, the total area of significant cold and hot classes (significance > 90%) was 18.4 and 22.6% of the total city area, respectively (Figs. 4a and 6).

The spatial pattern of hot and cold spots during the reference period and 2022 show both similarities and differences. For example, for both periods, cold spots are concentrated over the southeast, northwest, and southern areas of the city. However, for the reference period, a cold core was observed over the southwestern portion of the city, of which there is no trace in 2022. The arrangement of hot spots was concentrated over the northern half of central Donetsk during the reference period, while during 2022, hot spots were more scattered and "patchy," with a lower density over central parts of the city than during the reference period (Fig. 4a, b).

The LST fluctuates from a minimum of 5.5°C to a maximum of 8°C for the reference period, and in 2022 this temperature fluctuation is from 4 to 8°C. For the reference period, the maximum area (27.44%) is for the temperature class 7–7.5°C, while the maximum area in 2022 (31.82%) was for the temperature class 6–6.5°C (Fig. 4c, d). The curve for different temperature classes indicates that the frequency of low-temperature occurrences in 2022 was higher than that for the reference period (Fig. 7). When examining changes in UHII using the G_i^*UHII method, the UHII value for 2022 was 1.46°C, and that for the reference period was 1.53°C.

The UHII ranged from − 1.5 to 2.5°C during the reference period, while that in 2022 ranged from − 1.5 to 2°C (Fig. 4e, f). Areas with decreasing and increasing UHII were 25.24 and 74.77%, respectively, for the reference period, and 24.97 and 75.02%, respectively, in 2022–hence very similar (Fig. 8). Spatial changes of the UHII pattern show that there is a maximum increase in UHII over the northern half of central Donetsk, with expansion toward western, eastern, and southern parts of the city. Northwestern and southwestern parts of the city record maximum declines in UHII between the two study periods (Fig. 4e, f).

Mariupol city records significant cold and hot classes (significance > 90%) over 14.36 and 16.12% of the total city area, respectively (Figs. 5b and 6). In 2022, significant cold and hot classes (significance > 90%) cover 11.90 and 15.85% of the total city area, respectively (Figs. 5a and 6).

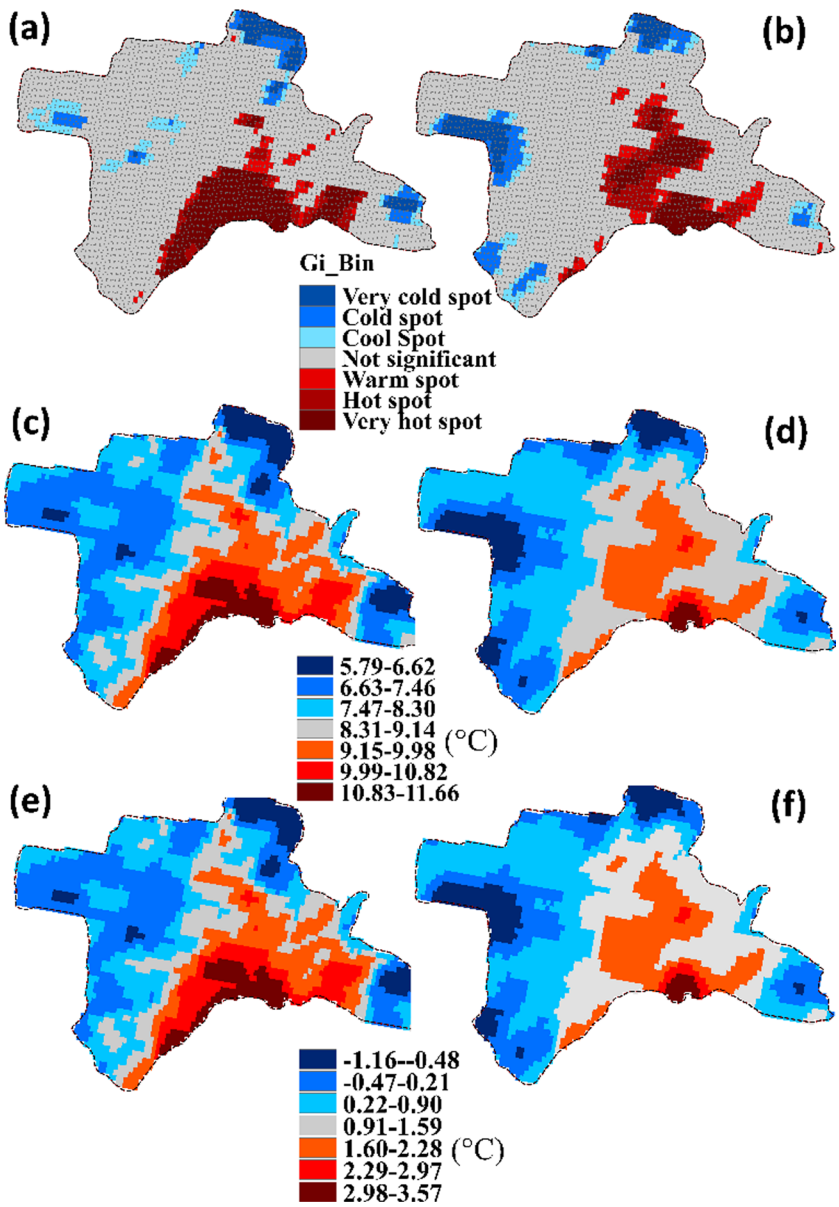


Fig. 5 Spatio-temporal distribution of hot spot analysis: **a** nighttime 2022, **b** nighttime reference period (LST), **c** nighttime 2022, **d** nighttime reference period and urban heat island intensity, **e** nighttime 2022, and **f** nighttime reference period for Mariupol city

The spatial pattern of cold and hot spots shows that the cold core over the western half of the city is stronger during the reference period than in 2022. During the reference period, hot spots extended from north to south, which then changed to a west–east extension in 2022 (Fig. 5a, b).

During the reference period, different areas of the city experienced variable LST values of between 6 and 13°C at night but were reduced to between 6 and 11°C in 2022 (Fig. 5c, d). The curve for different temperature classes indicates that the frequency of low-temperature occurrences in 2022 was higher than that for the reference period (Fig. 7). For the reference period, the largest area of the city (32.28%) recorded a temperature class of 9 to 10°C, but in 2022, the maximum area (60%) recorded a temperature class of 7 to 8°C (Fig. 5c, d).

Changes in the UHII using the G_i^*UHII method indicate nighttime values of 2.38 and 2.44°C for 2022 and the reference period, respectively. The UHII ranged from – 1.5 to 6°C during the reference period, while that in 2022 ranged from – 1.5 to 4°C (Fig. 5e, f). Areas with decreasing and increasing UHII were 16.75 and 83.25%, respectively, for the reference period, and 16.90 and 83.10%, respectively, in 2022—hence very similar (Fig. 8). Spatial changes of the UHII pattern show that there is a maximum increase (decrease) in UHII over the eastern half (western half) of Mariupol, visible for both periods (Fig. 5e, f).

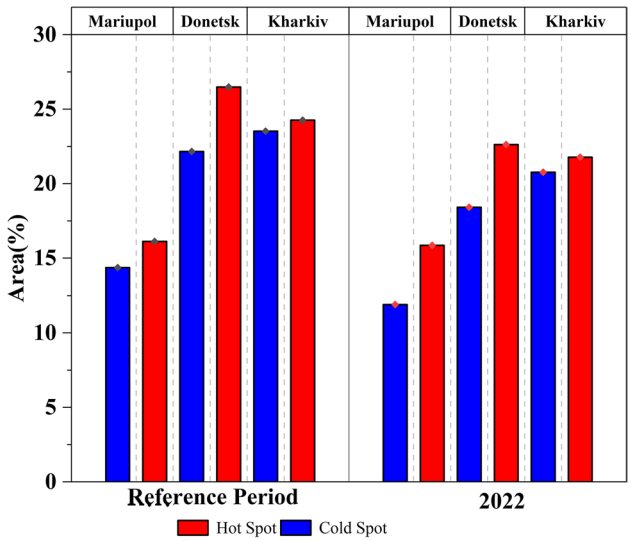


Fig. 6 Total area occupied by cold and hot spots (significance > 90%) during the night

The impact of war on air quality

AAI index results for all three cities show that there is a significant difference between the war year (2022) and the 3 years prior to the war (Fig. 9). In 2022, the maximum frequency of AAI tends toward positive values, while it is negatively skewed in earlier years. In Kharkiv, 53% of days during 2022 recorded positive AAI values, significantly higher than for previous years (24% in 2019; 13% in 2020; 36% in 2021) (Fig. 9). Index scores show a similar pattern: 2022 = − 0.20, and years 2019 to 2021 = − 0.74, − 1.02, and − 0.59, respectively (Fig. 9). A shift to more positive AAI values is indicative of higher concentrations of aerosol plumes, as was the case in 2021, and more particularly so in 2022. Results for Donetsk show that in 2022, 28% of days had positive AAI values, while earlier years had considerably fewer positive AAI days (7% in 2019; 5% in 2020, and 17% in 2021) (Fig. 9). The same pattern (i.e., % of days with positive AAI results) is recorded for Mariupol (33.5% of days in 2022 as opposed to 6.71, 2.22, and 2.72% for the years 2019 to 2021, respectively). AAI index scores similarly follow a consistent pattern for all three cities (Fig. 9).

Overall, the city experienced a − 2.7% decrease in mean CO values in 2022, compared with the mean for the three previous years when values ranged from 23.3% of days in 2022 to 26.6% of days in 2019 (Fig. 10). For Kharkiv, the annual CO value was lowest in 2022 (0.035 mol m^{-2}) and ranged from 0.035 mol m^{-2} in 2022 to 0.039 mol m^{-2} in 2021. For Donetsk, CO varies from the lowest value in 2022 (0.036 mol m^{-2}) to the highest value in 2019 (0.046 mol m^{-2}). Similarly, Mariupol had the lowest CO values in 2022 (0.038 mol m^{-2}),

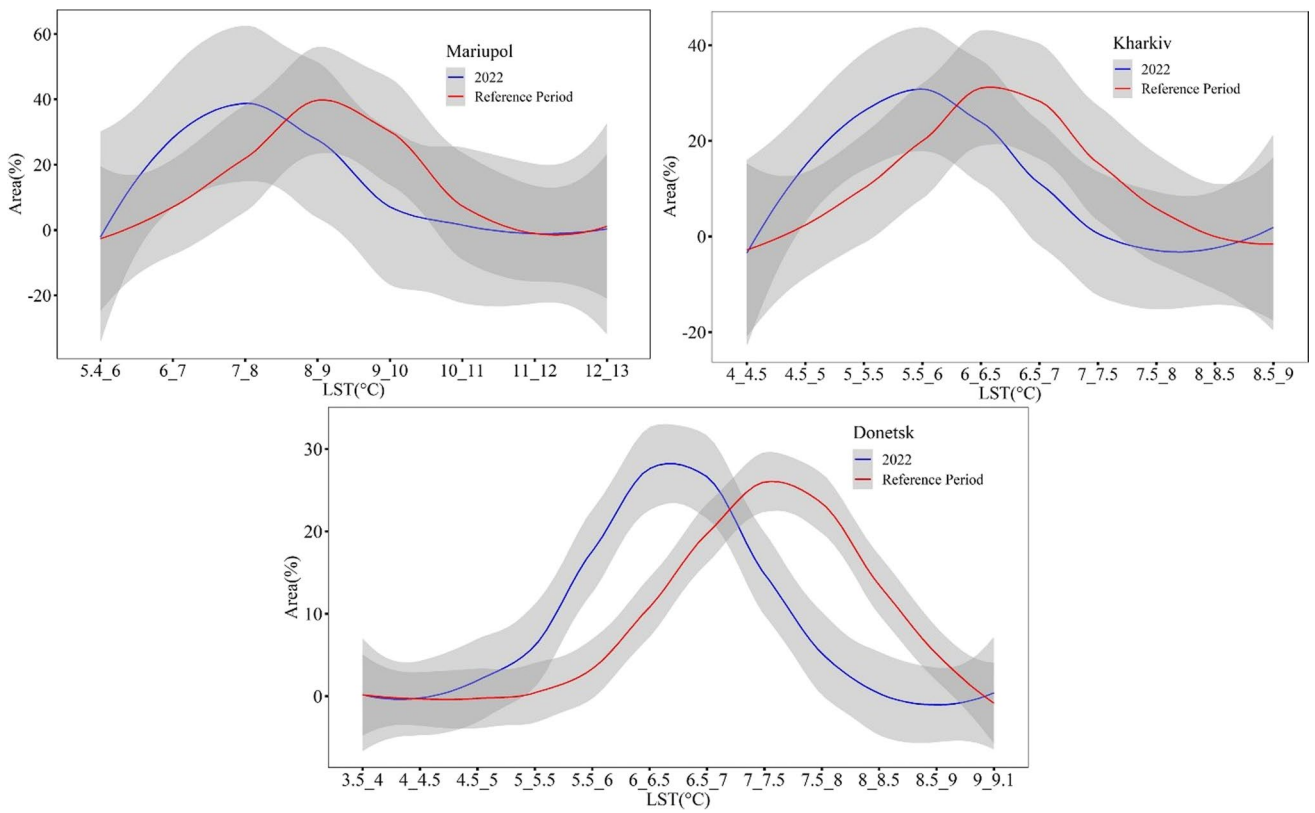


Fig. 7 Frequency of area located in different LST classes for 2022 and the reference period in the three cities

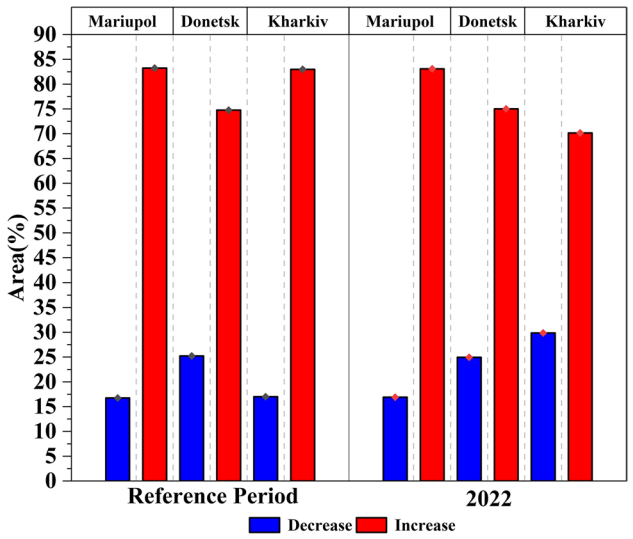


Fig. 8 Percentage areas with increasing and decreasing nighttime UHII, with maximum and minimum temperature UHI thresholds (°C) for the three cities

compared with a mean value of 0.042 mol m^{-2} for the 3 years prior (Fig. 10). There is thus a unanimous pattern across all three cities, showing reduced CO values in 2022.

Nighttime lights before and during the war

As might have been expected, nighttime light (NTL) values in 2022 were reduced in all three cities (by 21.3%), compared to values in earlier years. The mean NTL index value for Kharkiv in 2022 was 41.20 MJ m^{-2}, compared to an average of 138.3 MJ m^{-2} for the 3 years prior—this represents a 21.3% reduction in 2022 (Fig. 11). The mean NTL index value for Donetsk in 2022 was 42.70 MJ m^{-2}, compared to an average of 51.2 MJ m^{-2} for the 3 years prior—this represents a 4.3% reduction in 2022. The mean NTL index value for Mariupol in 2022 was 21.52 MJ m^{-2}, compared to an average of 78.1 MJ m^{-2} for the 3 years prior—this represents a 22.1% reduction in 2022.

Discussion

Our findings show that of the three cities investigated, Mariupol has the smallest area occupied by cold and hot spots during both the reference period and 2022. We postulate that the Black Sea has a moderating influence on the urban climate of Mariupol and likely helps regulate temperatures over the city. Past studies have similarly confirmed that water bodies (oceans, seas, lakes, and large rivers) may influence the behavior of UHIs. For instance, it has been confirmed that large rivers (Murakawa et al. 1991; Hathway and Sharples 2012; Moyer and Hawkins 2017) and sea breezes (e.g., He et al., 2020) have a cooling effect on adjacent cities (urban heat islands). Most notable is the overall decreased area of nighttime hot spots in 2022 compared to the reference period for all three cities. We thus propose that the recent war in Ukraine has likely played a role in reducing the area of nightly hot spots in these cities.

A large number of war-related refugees have emigrated from Ukraine, starting as early as February 2022 (Andrews et al. 2023). This migration of several million people, mainly to neighboring European countries, has been unprecedented since World War II (Bouchard et al. 2023). For example, during the first 2 months of the war, more than 3 million refugees entered Poland (Lee et al. 2023). Based on a report by the "Institute for System Statistical Studies" (Bouchard et al. 2023), an estimated 3.7–4.0 million people had fled the country by 15 March 2022. The number of refugees (10% of the country's total population) corresponds with an even higher number of internally displaced people (6.5 million by mid-March 2022, according to UNCHR) (Bouchard et al. 2023). Essentially, it equates to > 25% of the total population (including the urban population) having left their places of residence. The consequence of this is a likely higher percentage of economic downturn, although this is as yet difficult to quantify temporally.

Outmigration of people from urban areas and associated reduced economic activity is known to yield reduced heat budgets and air pollution in affected cities. For example, such scenarios have been quantified for the Beijing metropolis before and after the Chinese New Year, when nearly half of Beijing's population is estimated to depart the city each year (Zhang et al. 2015).

More recent studies have confirmed similar patterns in association with forced urban lockdowns associated with the COVID-19 pandemic, namely that LST and UHIs were reduced when compared with years prior to the pandemic (Parida et al. 2021; Kenawy et al. 2021; Roshan et al. 2021, 2022; Jamei et al. 2022; Jallu et al. 2022; Mijani et al. 2023).

Our study has demonstrated varying patterns of atmospheric pollution in Ukrainian cities in 2022, likely associated with the recent war. This includes reduced CO levels (by 3.3%) but increased AAI (by 27.2%). Carbon monoxide (CO) is known to be a major trace gas in urban environments, associated with biomass burning, fossil fuel combustion, and the atmospheric oxidation of methane and other hydrocarbons (Abonomi et al 2022; Opio et al. 2021). It is thus likely that with outmigration from the affected cities and despite the pollutants released through military activity, the net effect has been a reduction in such CO-emitting sources. Notably, the CO concentration in the investigated cities in 2022 is not too dissimilar to that in 2020. We

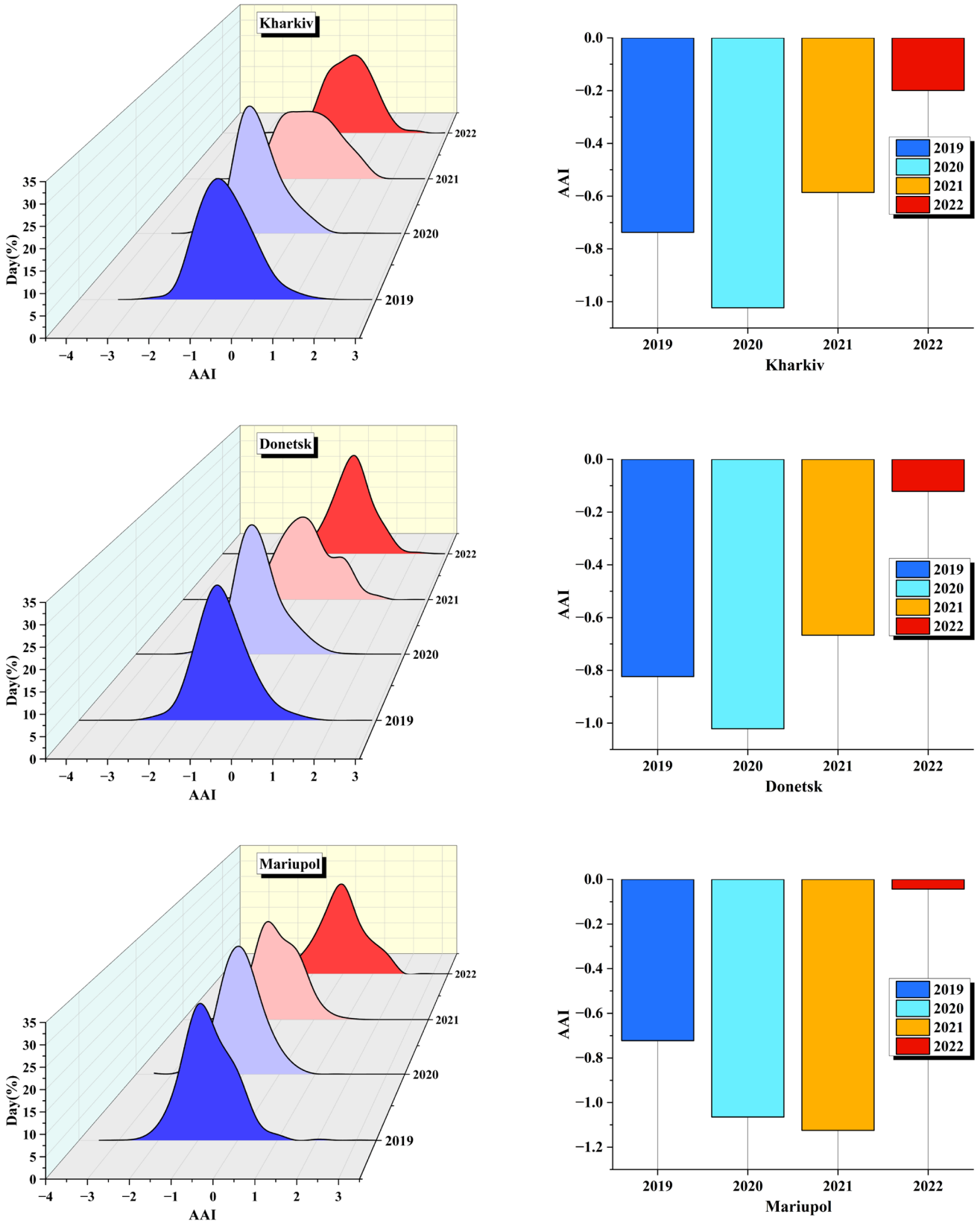


Fig. 9 Graphics on the left show % of days for given years with positive/negative AAI scores. The graphics on the right represent mean annual AAI values

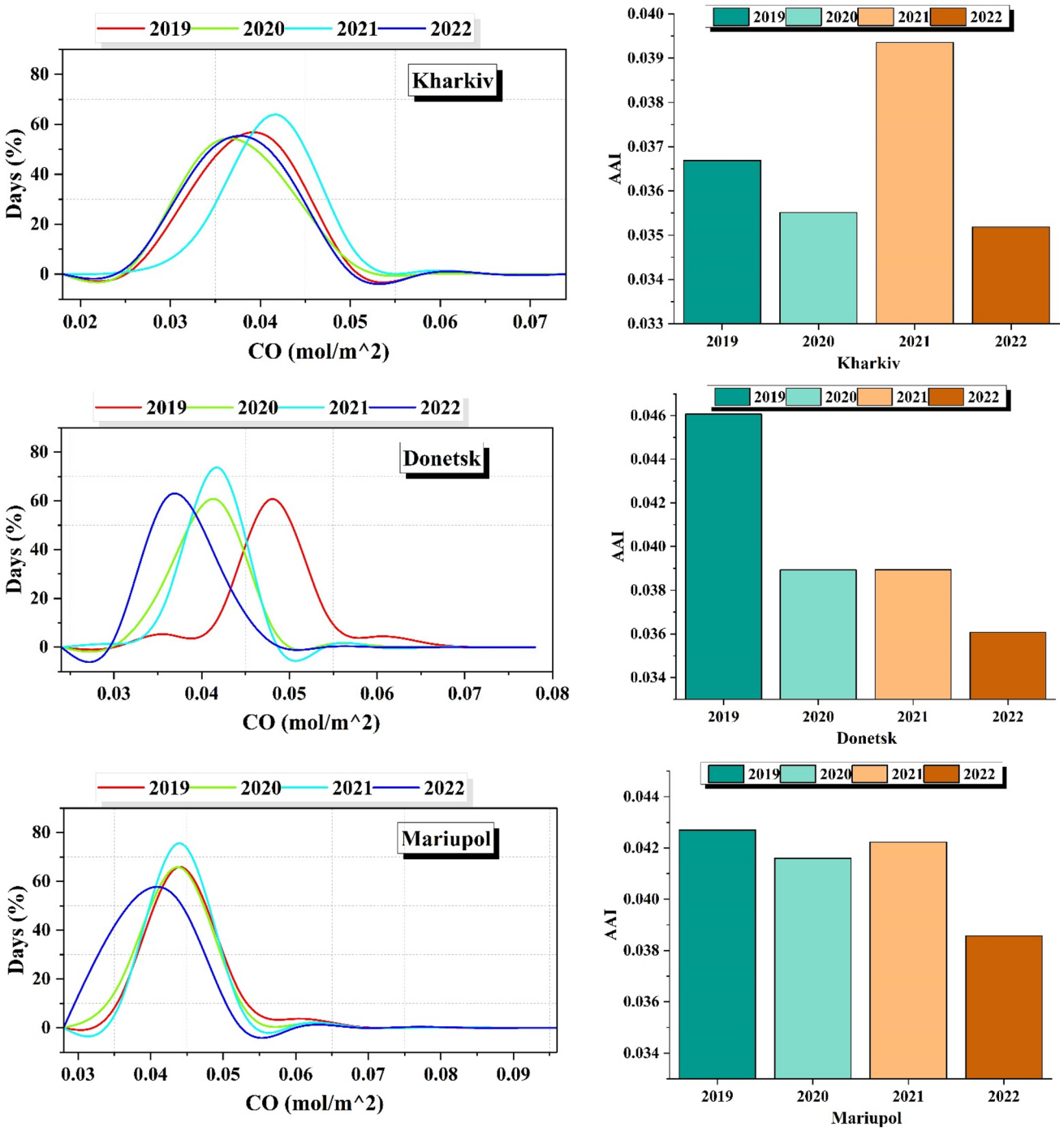


Fig. 10 Graphics on the left show % of days for given years with given CO values. The graphics on the right represent the mean annual CO values for the three cities

postulate that reduced CO levels in 2020 were related to the COVID-19 pandemic urban lockdown and hence reduced human activities, as was the case in many urban regions worldwide (Mahato and Ghosh 2020; Chen et al. 2020; Bray et al. 2021; Barua and Nath 2021; Cucciniello et al. 2022). In addition, it has already been demonstrated that NO_2 concentrations in Ukrainian cities have decreased by 10.7–27.3% due to the war (Zhang et al. 2023).

Increased concentrations of AAI in the atmosphere may indicate the presence of suspended UV-absorbing particles in the air, such as dust and smoke. It seems most likely (although difficult to prove quantitatively) that the destruction of

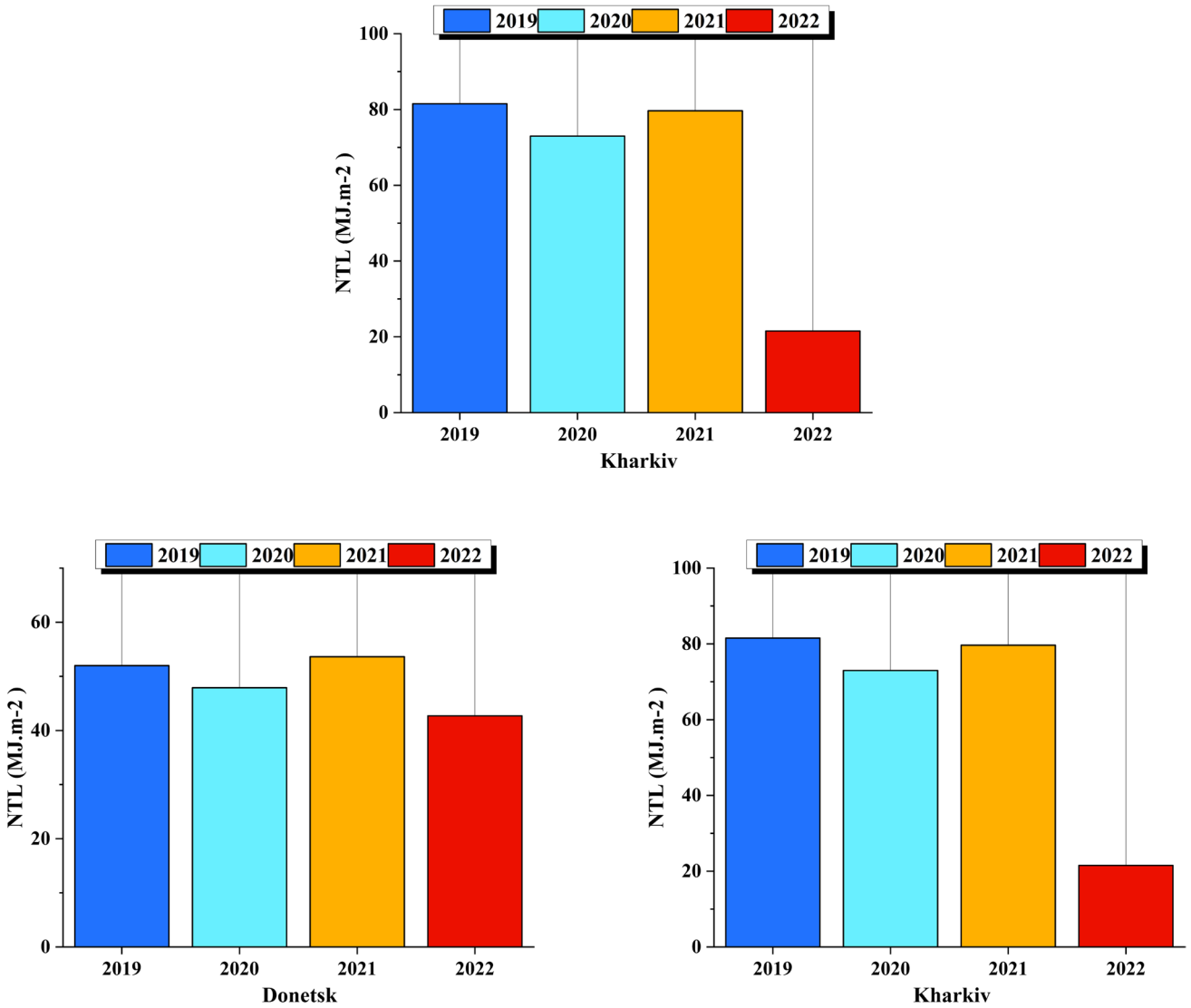


Fig. 11 Mean annual NTL values for the years 2019–2022 (2019–2021 representing pre-war years)

buildings (which leads to the production of dust) due to bombing, or the release of smoke from fires and military activities, has yielded a significant increase in AAI over eastern Ukrainian cities. This inference is also supported by a study demonstrating that the war in Ukraine has led to an increase in T550 concentration (Aerosol Optical Thickness) in the areas around Kiev (Neckel et al. 2022). Furthermore, Kiev's air quality has also been affected by increased O_3 and a 75% reduction in SO_2 concentration (Zalakeviciute et al. 2022). A growing concern has been that increased urban air pollution in association with bombing and fires may already have led to considerable health concerns (Zalakeviciute et al. 2022).

At this point, we acknowledge that the connection between war and reduced economic activity is one based on *reasonable assumptions* rather than quantitative information. An important factor that may help confirm the assumption made is the NTL value. The brightness of night lights is not only closely correlated with economic activities (e.g., Guo et al. 2020; Chen et al. 2023) but may also indicate the vulnerability of cities to natural disasters, such as floods, earthquakes (Yu et al., 2023), or the relationship between nighttime light and the incidence of deaths caused by COVID-19 (Zhang et al., 2023). In addition, warring parties may use such NTL to identify urban areas not yet destroyed and thus provide a measure for ongoing targets. The substantial reduction (16%) of NTL in our three investigated cities thus provides a good indication that economic/human activity was significantly reduced due to the war in 2022.

Conclusion

Some of the most significant consequences of war are the destruction of infrastructure, the economic downturn, and the deprivation of human well-being. In some cases, the urban fabric that has been built up over centuries may be destroyed in a matter of a few days or months. Recent studies have shown that the Russia–Ukraine war had a direct impact on atmospheric gas and aerosol concentrations in Ukraine. For instance, there has been a reduction in nitrogen dioxide (NO_2) (Zhang et al. 2023) and an increase in the concentration of T550 (Aerosol Optical Thickness) (Neckel et al. 2022) as a direct consequence of the war. This paper has demonstrated, through the use of remote sensing techniques, how urban climates (i.e., UHI, LST, and air quality) in eastern Ukraine have also been impacted by war.

As our findings show, there are differences in patterns of atmospheric pollution in these cities as a direct consequence of war. Such differences may be accounted for by varying levels of conflict and human outmigration across "space"—but these are difficult to quantify with precision. In addition, it is likely that other factors, such as regional synoptic patterns, topography, distance and proximity to water bodies, etc., have impacted some of our findings and may account for inter-city variability in observed patterns (see also Bernardino et al. 2021; Ghanghermeh et al. 2022; Yang et al. 2023; Yin et al. 2023). Urban air quality and associated human health implications associated with wars, such as the ongoing war in Ukraine, require ongoing research and media attention, particularly as this is a relatively underreported component of human conflict but indeed impacts lives.

Author contribution Gholamreza Roshan: conceptualization, methodology, validation, formal analysis, and writing—original draft preparation and supervision. Abdolazim Ghanghermeh: conceptualization, methodology, validation, formal analysis, software, and project administration. Reza Sarli: software, formal analysis, data curation, and visualization. Stefan Grab: conceptualization, methodology, and writing—review and editing. All authors read and approved the final manuscript.

Data Availability The datasets used during the current study are available from the corresponding author on reasonable request.

Declarations

Ethical approval There are no human subjects or animals in this article, and ethical approval is not applicable.

Consent to participate There are no human subjects or animals in this article, and consent to participate is not applicable.

Consent for publication Not applicable (this manuscript does not include any individual person's information). All authors have agreed to publish.

Conflict of interest The authors declare no conflict of interest.

References

Abonomi A, De Lacy T, Pyke J (2022) Environmental Impact of the Hajj. International Journal of Religious Tourism and Pilgrimage 10(1):12. https://doi.org/10.21427/nv9g-6c27. Available at: https://arrow.tudublin.ie/ijrtp/vol10/iss1/12

Ali M, Tariq S, Mahmood K, Haq ZU (2014) A study of aerosol properties over Lahore (Pakistan) by using AERONET data. Asia-Pac J Atmos Sci 50:153–162

Andrews J, Isański J, Nowak M, Sereda V, Vacroux A, Vakhitova H (2023) Feminized forced migration: Ukrainian war refugees. Women's Stud Int Forum 99:102756. https://doi.org/10.1016/j.wsif.2023.102756

Apraku A, Gyampoh BA, Morton JF, Karikari AB (2023) Water security in rural Eastern Cape, SA: interrogating the impacts of politics and climate change. Sci Afr 19:e01493

Arellano B, Roca J (2021) Remote sensing and night time urban heat island. the International Archives of the Photogrammetry, Remote Sensing and Spatial Information Sciences/International Archives of the Photogrammetry, Remote Sensing and Spatial Information Sciences, XLIII-B3-2021, 15–22. https://doi.org/10.5194/isprs-archives-xliii-b3-2021-15-2021

Asfew M, Mitiku F, Gemechu A, Bekele Y, Lemma T (2023) Do climate change and political instability affect crop production in sub-Saharan Africa countries? J Afr Agric Food Res 12:100576

Barua S, Nath SD (2021) The impact of COVID-19 on air pollution: evidence from global data. J Clean Prod 298:126755

BBC News (2022) COP27_ War causing huge release of climate warming gas claims Ukraine. Available online: https://www.bbc.com/news/science-environment-63625693. Accessed 14 Nov 2022

Beria P, Lunkar V (2021) Presence and mobility of the population during the first wave of Covid-19 outbreak and lockdown in Italy. Sustain Cities Soc 65:102616

Bernardino AD, Iannarelli AM, Casadio S, Perrino C, Barnaba F, Tofful L, Campanelli M, Liberto LD, Mevi G, Siani AM, Cacciani M (2021) Impact of synoptic meteorological conditions on air quality in three different case studies in Rome Italy. Atmos Pollut Res 12(4):76–88

Bilal M, Mhawish A, Nichol J, Qiu Z, Nazeer M, Ali M, Leeuw G, Levy R, Wang Y, Chen Y, Wang L, Shi Y, Bleiweiss M, Mazhar U, Atique L, Ke S (2021) Air pollution scenario over Pakistan: characterization and ranking of extremely polluted cities using long-term concentrations of aerosols and trace gases. Remote Sens Environ 264:112617

Bouchard JP, Stiegler N, Padmanabhanunni A, Pretorius TB (2023) Psychotraumatology of the war in Ukraine: the question of the psychological care of victims who are refugees or who remain in Ukraine. Ann Méd-Psychol Rev Psychiatrique 181(1):12–15

Bray CD, Nahas A, Battye WH, Aneja VP (2021) Impact of lockdown during the COVID-19 outbreak on multi-scale air quality. Atmos Environ 254:118386

Buhaug H, Benjaminsen TA, Gilmore EA, Hendrix CS (2023) Climate-driven risks to peace over the 21st century. Clim Risk Manag 39:100471

Burnett M, Mach KJ (2021) A "precariously unprepared" Pentagon? Climate security beliefs and decision-making in the U.S. military. Glob Environ Chang 70:102345

Chen Z, Hao X, Zhang X, Chen F (2020) Have traffic restrictions improved air quality? A shock from COVID-19. J Clean Prod 279:123622

Chen W, Xu Q, Zhao K, Hao L, Pu C, Yuan S, Chui S, Zhao H, Yang K (2023) Spatiotemporal expansion modes of urban areas on the Loess Plateau from 1992 to 2021 based on nighttime light images. Int J Appl Earth Obs Geoinf 118:103262

Correia Filho WL, de Barros Santiago D, de Oliveira-Júnior JF, da Silva Junior CA (2019) Impact of urban decadal advance on land use and land cover and surface temperature in the city of Maceió, Brazil. Land Use Policy 87:104026. https://doi.org/10.1016/j.landusepol.2019.104026

Correia Filho WL, de Barros Santiago D, de Oliveira-Júnior JF, da Silva Junior CA, da Silva Oliveira SR, da Silva EB, Teodoro PE (2021) Analysis of environmental degradation in Maceió-Alagoas, Brazil via orbital sensors: a proposal for landscape intervention based on urban afforestation. Remote Sens Appl: Soc Environ 24:100621

Croft TA (1978) Nighttime images of the Earth from space. Sci Am 239:86–98

Cucciniello R, Raia L, Vasca E (2022) Air quality evaluation during COVID-19 in Southern Italy: the case study of Avellino city. Environ Res 203:111803

da SilvaEspinoza N, dos Santos CA, de Oliveira MBL, Silva MT, Santos CAG, da Silva RM, Mishra M, Ferreira RR (2023) Assessment of urban heat islands and thermal discomfort in the Amazonia biome in Brazil: a case study of Manaus city. Build Environ 227:109772 (**Part 1**)

Deren L, Xi L (2015) An overview on data mining of nighttime light remote sensing. Acta Geodaet Cartographica Sin 44(6):591–601

Donnelly K, Ha ML, Cooley H, Morrison J (2012) Water as a casualty of conflict: threats to business and society in high-risk areas. Pacific Institute, United Nations Global Compact

Elvidge CD, Baugh K, Zhizhin M, Hsu FC, Ghosh T (2017) VIIRS night-time lights. Int J Remote Sens 38:5860–5879

Elvidge CD, Zhizhin M, Ghosh T, Hsu FC, Taneja J (2021) Annual time series of global VIIRS nighttime lights derived from monthly averages: 2012 to 2019. Remote Sens 13(5):922

ESRI (2018) How hot spot analysis: Getis-Ord Gi* (Spatial Statistics) works [WWW Document]. URL http://pro.arcgis.com/en/pro-app/tool-reference/spatialstatistics/h-how-hot-spot-analysis-getis-ord-gispatial-stati.htm (accessed 2.21.18)

Garajeh MK, Haji F, Tohidfar M, Sadeqi A, Ahmadi R, Kariminejad N (2024) Spatiotemporal monitoring of climate change impacts on water resources using an integrated approach of remote sensing and Google Earth Engine. Sci Rep 14(1). https://doi.org/10.1038/s41598-024-56160-9

Garfin G, Falk DA, O'Connor CD, Jacobs K, Sagarin RD, Haverland AC, Haworth A, Baglee A, Weiss J, Overpeck J, Zuñiga-Terán AA (2021) A new mission: mainstreaming climate adaptation in the US Department of Defense. Clim Serv 22:100230

Georgiana G, Uritescu B (2018) Spatial hotspot analysis of Bucharest's Urban Heat Island (UHI) using Modis Data. Ann Valahia Univ Targoviste Geogr Ser 18(1):14–22

Ghanghermeh A, Roshan GH, Halabian A (2022) Projecting spatiotemporal variations of sunshine duration with regards to climate change in Iran as a step towards clean energy. Sustain Energy Technol Assessments 53:102630 (**Part C**)

Gleick PH (2019) Water as a weapon and casualty of conflict: freshwater and International Humanitarian Law. Water Resour Manage 33(5):1737–1751

Guo Y, Yu W, Chen Z, Zou R (2020) Impact of high-speed rail on urban economic development: An observation from the Beijing-Guangzhou line based on night-time light images. Socioecon Plann Sci 72:100905

Hammer MS, Martin RV, van Donkelaar A, Buchard V, Torres O, Ridley DA, Spurr RJD (2016) Interpreting the ultraviolet aerosol index observed with the OMI satellite instrument to understand absorption by organic aerosols: implications for atmospheric oxidation and direct radiative effects. Atmos Chem Phys 16:2507–2523

Hathway EA, Sharples S (2012) The interaction of rivers and urban form in mitigating the urban heat island effect: a UK case study. Build Environ 58:14–22

He BJ (2018) Potentials of meteorological characteristics and synoptic conditions to mitigate urban heat island effects. Urban Clim 24:26–33

Wang Z, Xiong X, Fulbright J, Lei N (2017) VIIRS day/night band radiometric calibration stability monitoring using the moon. J Geophys Res Atmos 122(11):5616

He BJ, Ding L, Prasad D (2020) Relationships among local-scale urban morphology, urban ventilation, urban heat island and outdoor thermal comfort under sea breeze influence. Sustain Cities Soc 60:102289

Herndon JM (2019) World War II holds the key to understanding global warming and the challenge facing science and society. J Geogr Environ Earth Sci Int 23(4):1–13

Hou H, Su H, Yao C, Wang ZH (2023) Spatiotemporal patterns of the impact of surface roughness and morphology on urban heat island. Sustain Cities Soc 92:104513

Huang C, Hong S, Niu X, Wu Q, Zhong Y, Yang H, Zhang H (2023) Mapping of nighttime light trends and refugee population changes in Ukraine during the Russian-Ukrainian War. Front Environ Sci 11:1055100

Husain T (1998) Terrestrial and atmospheric environment during and after the Gulf War. Environ Int 24:189–196

Husni E, Prayoga GA, Tamba JD, Retnowati Y, Fauzandi FI, Yusuf R, Yahya BN (2022) Microclimate investigation of vehicular traffic on the urban heat island through IoT-based device. Heliyon 8(11):e11739

Jallu SB, Shaik RU, Srivastav R, Pignatta G (2022) Assessing the effect of covid-19 lockdown on surface urban heat island for different land use/cover types using remote sensing. Energy Nexus 5:100056

Jamei E, Jamei Y, Seyedmahmoudian M, Horan B, Mekhilef S, Stojcevski A (2022) Investigating the impacts of COVID-19 lockdown on air quality, surface Urban Heat Island, air temperature and lighting energy consumption in City of Melbourne. Energ Strat Rev 44:100963

Jayaram D, Brisbois MC (2021) Aiding or undermining? The military as an emergent actor in global climate governance. Earth Syst Gov 9:100107

Kenawy AM, Lopez-Moreno JI, McCabe MF, Domínguez-Castro F, Peña-Angulo D, Gaber IM et al (2021) The impact of COVID-19 lockdowns on surface urban heat island changes and air-quality improvements across 21 major cities in the Middle East. Environ Pollut 228:117802

Khosravian J, Qureshi S, Rostamzadeh S, Moradi B, Derakhshesh P, Yousefi S, Jamali K, Ahmadi R, Nickravesh F (2024) Evaluating the feasibility of constructing shopping centers on urban vacant land through a spatial multi-criteria decision-making model. Front Sustain Cities 6. https://doi.org/10.3389/frsc.2024.1373331

Kooreman ML, Stammes P, Trees V, Sneep M, Tilstra LG, De Graaf M, Zweers DCS, Wang P, Tuinder ONE, Veefkind JP (2020) Effects of clouds on the UV Absorbing Aerosol Index from TROPOMI. Atmospheric Measurement Techniques 13(12):6407–6426. https://doi.org/10.5194/amt-13-6407-2020

Kordi F, Yousefi H (2022) Crop classification based on phenology information by using time series of optical and synthetic-aperture radar images. Remote Sens Appl 27:100812. https://doi.org/10.1016/j.rsase.2022.100812

Kumar A, Mukherjee M, Goswami A (2023) Inter-seasonal characterization and correlation of surface Urban Heat Island (SUHI) and Canopy Urban Heat Island (CUHI) in the urbanized environment of Delhi. Remote Sens Appl: Soc Environ 30:100970

Lee ACK, Khaw FM, Lindman AES, Juszczyk G (2023) Ukraine refugee crisis: evolving needs and challenges. Public Health 217:41–45

Li L, Li J, Peng L, Wang X, Sun S (2023) Spatiotemporal evolution and influencing factors of land-use emissions in the Guangdong-Hong Kong-Macao Greater Bay Area using integrated nighttime light datasets. Sci Total Environment 893:164723. https://doi.org/10.1016/j.scitotenv.2023.164723

Lin Y, Wang Z, Jim CY, Li J, Deng J, Liu J (2020) Water as an urban heat sink: Blue infrastructure alleviates urban heat island effect in mega-city agglomeration. J Clean Prod 262:121411

Ma HY, Li HJ, Zhang M, Dong X (2022) Impact of cropland degradation in the rural–urban fringe on urban heat island and heat stress during summer heat waves in the Yangtze River Delta. Adv Clim Chang Res 13(2):240–250

Mahato S, Ghosh KG (2020) Short-term exposure to ambient air quality of the most polluted Indian cities due to lockdown amid SARS-CoV-2. Environ Res 188:109835

Mahmoud SH, Gan TY (2018) Long-term impact of rapid urbanization on urban climate and human thermal comfort in hot-arid environment. Build Environ 142:83–100

Mansourihanis O, Tilaki MJM, Yousefian S, Zaroujtaghi A (2023) A computational geospatial approach to assessing land-use compatibility in urban planning. Land 12(11):2083. https://doi.org/10.3390/land12112083

Mijani N, Firozjaei MK, Mijani M, Khodabakhshi A, Qureshi S, Arsanjani JJ, Alavipanah SK (2023) Exploring the effect of COVID-19 pandemic lockdowns on urban cooling: A tale of three cities. Adv Space Res 71(1):1017–1033. https://doi.org/10.1016/j.asr.2022.09.052

Mills S, Weiss S, Liang C (2013) VIIRS day/night band (DNB) stray light characterization and correction. Proceedings of SPIE, the International Society for Optical Engineering/Proceedings of SPIE. https://doi.org/10.1117/12.2023107

Morris KI, Chan A, Morris KJ, Ooi MCG, Oozeer MY, Abakr YA, Mohd Nadzir MS, Mohammed IY, Al-Qrimli HF (2017) Impact of urbanization level on the interactions of urban area, the urban climate, and human thermal comfort. Appl Geogr 79:50–72

Mortoja MG, Yigitcanlar T (2022) Understanding political bias in climate change belief: a public perception study from South East Queensland. Land Use Policy 122:106350

Moyer AN, Hawkins TW (2017) River effects on the heat island of a small urban area. Urban Clim 21:262–277

Murakawa S, Sekine T, Narita KI, Nishina D (1991) Study of the effects of a river on the thermal environment in an urban area. Energy Build 15–16:993–1001

Neckel A, Santosh M, Bodah BW, Maculan LS, Pinto D, Korcelski C, Toscan PC, Cambrussi LP, Caino IC, Moro LD (2022) Using the Sentinel-3B satellite in geospatial analysis of suspended aerosols in the Kiev Ukraine Region. Sustainability 14:16357

Nemati M, Ebrahimi B, Nemati F (2020) Assessment of Iranian nurses' knowledge and anxiety toward COVID-19 during the current outbreak in Iran. Archives of Clinical Infectious Diseases, 15(COVID-19). https://doi.org/10.5812/archcid.102848

Ngarambe J, Oh JW, Su MA, Santamouris M, Yun GY (2021) Influences of wind speed, sky conditions, land use and land cover characteristics on the magnitude of the urban heat island in Seoul: An exploratory analysis. Sustain Cities Soc 71:102953

Opio R, Mugume I, Nakatumba-Nabende J (2021) Understanding the trend of NO_2, SO_2 and CO over East Africa from 2005 to 2020. Atmosphere 12:1283

Parida BR, Bar S, Kaskaoutis D, Pandey AC, Polade SD, Goswami S (2021) Impact of COVID-19 induced lockdown on land surface temperature, aerosol, and urban heat in Europe and North America. Sustain Cities Soc 75:103336

Pereira P, Bašić F, Bogunovic I, Barcelo D (2022) Russian-Ukrainian war impacts the total environment. Sci Total Environ 837:155865

Prins K (2022) War in Ukraine, and extensive forest damage in central Europe: Supplementary challenges for forests and timber or the beginning of a new era? Forest Policy and Economics 140:102736. https://doi.org/10.1016/j.forpol.2022.102736

Qiang Y, Huang QX, Xu JW (2020) Observing community resilience from space: Using nighttime lights to model economic disturbance and recovery pattern in natural disaster. Sustain Cities Soc 57:102115

Qin M, Su CW, Umar M, Lobonţ OR, Manta AG (2023) Are climate and geopolitics the challenges to sustainable development? Novel evidence from the global supply chain. Econ Anal Policy 77:748–763

Racioppi F, Rutter H, Nitzan D, Borojevic A, Carr Z, Grygaski TJ, Jarosińska D, Netanyahu S, Schmoll O, Stuetzle K, Den Akker AV, Kluge HHP (2022) The impact of war on the environment and health: implications for readiness, response, and recovery in Ukraine. Lancet 400(10356):871–873

Ramírez C, Durón RM (2022) The Russia-Ukraine war could bring catastrophic public-health challenges beyond COVID-19. Int J Infect Dis 120:44–45

Rawtani D, Gupta G, Khatri N, Rao PK, Hussain CM (2022) Environmental damages due to war in Ukraine: a perspective. Sci Total Environ 850:157932

Rodríguez-Urrego D, Rodríguez-Urrego L (2020) Air quality during the COVID-19: PM2.5 analysis in the 50 most polluted capital cities in the world. Environ Pollut 266:115042. https://doi.org/10.1016/j.envpol.2020.115042

Roshan G, Sarli R, Grab SW (2021) The case of Tehran's urban heat island, Iran: impacts of urban "lockdown" associated with the COVID-19 pandemic. Sustain Cities Soc 75:103263

Roshan GH, Sarli R, Fitchett JM (2022) Urban heat island and thermal comfort of Esfahan City (Iran) during COVID-19 lockdown. J Clean Prod 352:131498

Rudke AP, Martins JA, Hallak R, Martins LD, de Almeida DS, Beal A, Freitas ED, Andrade MF, Koutrakis P, Albuquerque TTA (2023) Evaluating TROPOMI and MODIS performance to capture the dynamic of air pollution in São Paulo state: a case study during the COVID-19 outbreak. Remote Sens Environ 289:113514

Schillinger J, Özerol G, Heldeweg M (2022) A social-ecological systems perspective on the impacts of armed conflict on water resources management: case studies from the Middle East. Geoforum 133:101–116

Selby J (2019) Climate change and the Syrian civil war, Part II: the Jazira's agrarian crisis. Geoforum 101:260–274

Shumilova O, Tockner K, Sukhodolov A, Khilchevskyi V, Meester L, Stepanenko S, Trokhymenko G, Hernández-Agüero J, Gleick P (2023) Impact of the Russia-Ukraine armed conflict on water resources and water infrastructure. Nat Sustain 6:578–586

Sirizi ME, Zirvani ET, Esmailzadeh A, Khosravian J, Ahmadi R, Mijani N, Soltannia R, Arsanjani JJ (2023) A scenario-based multi-criteria decision-making approach for allocation of pistachio processing facilities: a case study of Zarand Iran. Sustainability 15(20):15054. https://doi.org/10.3390/su152015054

Söder R (2023) Climate change, security and military organizations: changing notions in the Swedish armed forces. Earth Syst Gov 15:100169

Sovacool BK, Baum C, Low S (2023) The next climate war? Statecraft, security, and weaponization in the geopolitics of a low-carbon future. Energ Strat Rev 45:101031

The United Nations Satellite Centre (UNOSAT) (2022). Available online: https://unitar.org/maps/all-maps?page=2. Accessed 28 Jun 2022

United Nations Environment Programme (2022) The environmental impact of the conflict in Ukraine: a preliminary review. Nairobi, Kenya. Available at: https://wedocs.unep.org/20.500.11822/40746. Accessed 21 Jun 2024

Vukmirović ZB, Unkašević M, Lazić L, Tošić I (2001) Regional air pollution caused by a simultaneous destruction of major industrial sources in a war zone. The case of April Serbia in 1999. Atmos Environ 35:2773–2782

Watts C, Conger H (2022) Climate change and national security. Orbis 66(2):159–165

Wu B, Yang C, Wu Q, Wang C, Wu J, Yu B (2023) A building volume adjusted nighttime light index for characterizing the relationship between urban population and nighttime light intensity. Comput Environ Urban Syst 99:101911

Yale Environment 360 (2022) Collateral damage: the environmental cost of the Ukraine War. Published at the Yale School of the Environment. Access online: https://e360.yale.edu/features/ukraine-russia-war-environmental-impact. Accessed 29 Aug 2022

Yang Y, Guo M, Wang L, Zong L, Liu D, Zhang W, Wang M, Wan B, Guo Y (2023) Unevenly spatiotemporal distribution of urban excess warming in coastal Shanghai megacity, China: roles of geophysical environment, ventilation and sea breezes. Build Environ 235:110180

Yin S, Hua J, Ren C, Liu S, Lin H, Huang S, Wang K, Ma J, Xiao Y (2023) Impact of synoptic condition on urban microclimate variation: a measurement study in a humid subtropical city during summer season. Urban Clim 47:101350

Yu J, Zhou W, Jiang L, Yan W, Liu X (2023) Design seismic track irregularity for highspeed railways. Earthquake Engineering and Structural Dynamics/Earthquake Engineering & Structural Dynamics 52(15):4865–4883. https://doi.org/10.1002/eqe.3990

Zalakeviciute R, Vasquez R, Bayas D, Buenano A, Mejia D, Zegarra R, Diaz V, Lamb B (2020) Drastic improvements in air quality in Ecuador during the COVID-19 outbreak. Aerosol Air Qual Res 20:1783–1792

Zalakeviciute R, Mejia D, Alvarez H, Bermeo X, Bonilla-Bedoya S, Rybarczyk Y, Lamb B (2022) War impact on air quality in Ukraine. Sustainability 14:13832

Zhang J, Wu L, Yuan F, Dou J, Miao S (2015) Mass human migration and Beijing's urban heat island during the Chinese New Year holiday. Sci Bull 60(11):1038–1041

Zhang W, Cui Y, Wang J, Wang C, Streets DG (2020) How does urbanization affect CO_2 emissions of central heating systems in China? An assessment of natural gas transition policy based on nighttime light data. J Clean Prod 276:123188

Zhang C, Hu Q, Su W, Xing C, Liu C (2023) Satellite spectroscopy reveals the atmospheric consequences of the 2022 Russia-Ukraine war. Sci Total Environ 869:161759. https://doi.org/10.1016/j.scitotenv.2023.161759

Zhou D, Zhao S, Liu S, Zhang L, Zhu C (2014) Surface urban heat island in China's 32 major cities: spatial patterns and drivers. Remote Sens Environ 152:51–61

Publisher's Note Springer Nature remains neutral with regard to jurisdictional claims in published maps and institutional affiliations.

Springer Nature or its licensor (e.g. a society or other partner) holds exclusive rights to this article under a publishing agreement with the author(s) or other rightsholder(s); author self-archiving of the accepted manuscript version of this article is solely governed by the terms of such publishing agreement and applicable law.